detectors for setting the wavelength for optimized anomalous-scattering applications.

An area-detector development is the so-called pixel detector. This is made of silicon cells, each 'bump bonded' onto associated individual electronic readout chains. Thus, extremely high count rates are possible, and large area arrays of resolution elements may be conceived at a cost. These devices can then combine the attributes of large image-plate sensitive areas with the fast readout of CCDs, along with high count-rate capability and so on. Devices and prototypes are being developed at Princeton/Cornell (Eikenberry *et al.*, 1998), Berkeley/San Diego (Beuville *et al.* 1997), Imperial College, London (Hall, 1995), and by Oxford Instruments and the Rutherford Appleton Laboratory ('IMPACT' detector programme).

8.1.7. SR monochromatic and Laue diffraction geometry

In the utilization of SR, both Laue and monochromatic modes are important for data collection. The unique geometric and spectral properties of SR render the treatment of diffraction geometry different from that for a conventional X-ray source.

8.1.7.1. *Laue geometry: sources, optics, sample reflection bandwidth and spot size*

Laue geometry involves the use of the polychromatic SR spectrum as transmitted through the beryllium window that is used to separate the apparatus from the machine vacuum. There is useful intensity down to a wavelength minimum of $\sim\lambda_c/5$, where λ_c is the critical wavelength of the magnet source. The maximum wavelength is typically $\geq$3 Å; however, if the crystal is mounted in a capillary, then the glass absorbs the wavelengths beyond ~2.5 Å.

The bandwidth can be limited somewhat under special circumstances. A reflecting mirror at grazing incidence can be used for two purposes. First, the minimum wavelength in the beam can be sharply defined to aid the accurate definition of the Laue spot multiplicity. Second, the mirror can be used to focus the beam at the sample. The maximum-wavelength limit can be truncated by use of aluminium absorbers of varying thickness or a transmission mirror (Lairson & Bilderback, 1982; Cassetta *et al.*, 1993).

The measured intensity of individual Laue diffraction spots depends on the wavelength at which they are stimulated. The problem of wavelength normalization is treated by a variety of methods. These include:

(i) use of a monochromatic reference data set;

(ii) use of symmetry equivalents in the Laue data set recorded at different wavelengths;

(iii) calibration with a standard sample, such as a silicon crystal.

Each of these methods produces a 'λ curve' describing the relative strength of spots measured at various wavelengths. The methods rely on the incident spectrum being smooth and stable with time. The bromine and silver *K* absorption edges, in AgBr photographic film, lead to discontinuities in the λ-curve. Hence, the λ-curve is usually split up into wavelength regions, for example $\lambda_{\min}$ to 0.49 Å, 0.49 to 0.92 Å, and 0.92 Å to $\lambda_{\max}$. Other detector types have different discontinuities, depending on the material making up the X-ray absorbing medium. Most Laue diffraction data now recorded on CCDs or IPs. The greater sensitivity of these detectors (expressed as the DQE), especially for weak signals, has greatly increased the number of Laue exposures recordable per crystal. Thus, multiplet deconvolution procedures, based on the recording of reflections stimulated at different wavelengths and with different relative intensities, have become possible (Campbell & Hao, 1993; Ren & Moffat, 1995*b*). Data quality and completeness have improved considerably.

The production and use of narrow-bandpass beams, *e.g.* $\delta\lambda/\lambda \leq 0.2$, may be of interest for enhancing the signal-to-noise ratio. Such bandwidths can be produced by a combination of a reflection mirror used in tandem with a transmission mirror. Alternatively, an X-ray undulator of 10–100 periods should ideally yield a bandwidth behind a pinhole of $\delta\lambda/\lambda \simeq 0.1$–$0.01$. In these cases, wavelength normalization is more difficult, because the actual spectrum over which a reflection is integrated is rapidly varying in intensity; nevertheless, high-order Chebychev polynomials are successful (Ren & Moffat, 1995*a*).

The spot bandwidth is determined by the mosaic spread and horizontal beam divergence (since $\gamma_H > \gamma_V$) as

$$(\delta\lambda/\lambda) = (\eta + \gamma_H)\cot\theta, \tag{8.1.7.1}$$

where η is the sample mosaic spread, assumed to be isotropic, γ_H is the horizontal cross-fire angle, which in the absence of focusing is $(x_H + \sigma_H)/P$, where x_H is the horizontal sample size, σ_H is the horizontal source size and P is the sample to the tangent-point distance. This is similar for γ_V in the vertical direction. Generally, at SR sources, σ_H is greater than σ_V. When a focusing-mirror element is used, γ_H and/or γ_V are convergence angles determined by the focusing distances and the mirror aperture.

The size and shape of the diffraction spots vary across the detector image plane. The radial spot length is given by convolution of Gaussians as

$$\left(L_R^2 + L_c^2\sec^2 2\theta + L_{\rm PSF}^2\right)^{1/2} \tag{8.1.7.2}$$

and tangentially by

$$\left(L_T^2 + L_c^2 + L_{\rm PSF}^2\right)^{1/2}, \tag{8.1.7.3}$$

where L_c is the size of the X-ray beam (assumed to be circular) at the sample, $L_{\rm PSF}$ is the detector point spread factor,

$$L_R = D\sin(2\eta + \gamma_R)\sec^2 2\theta, \tag{8.1.7.4}$$

$$L_T = D(2\eta + \gamma_T)\sin\theta\sec 2\theta, \tag{8.1.7.5}$$

and

$$\gamma_R = \gamma_V\cos\psi + \gamma_H\sin\psi, \tag{8.1.7.6}$$

$$\gamma_T = \gamma_V\sin\psi + \gamma_H\cos\psi, \tag{8.1.7.7}$$

where ψ is the angle between the vertical direction and the radius vector to the spot (see Andrews *et al.*, 1987). For a crystal that is not too mosaic, the spot size is dominated by L_c and $L_{\rm PSF}$. For a mosaic or radiation-damaged crystal, the main effect is a radial streaking arising from η, the sample mosaic spread.

8.1.7.2. *Monochromatic SR beams: optical configurations and sample rocking width*

A wide variety of perfect-crystal monochromator configurations are possible and have been reviewed by various authors (Hart, 1971; Bonse *et al.*, 1976; Hastings, 1977; Kohra *et al.*, 1978). Since the reflectivity of perfect silicon and germanium is effectively 100%, multiple-reflection monochromators are feasible and permit the tailoring of the shape of the monochromator resolution function, harmonic rejection and manipulation of the polarization state of the beam. Two basic designs are in common use. These are the bent single-crystal monochromator of triangular shape (Fig. 8.1.4.1*a*) and the double-crystal monochromator (Fig. 8.1.4.1*b*).

8.1.7.2.1. *Curved single-crystal monochromator*

In the case of the single-crystal monchromator, the actual curvature employed is very important in the diffraction geometry. For a point source and a flat monochromator crystal, there is a

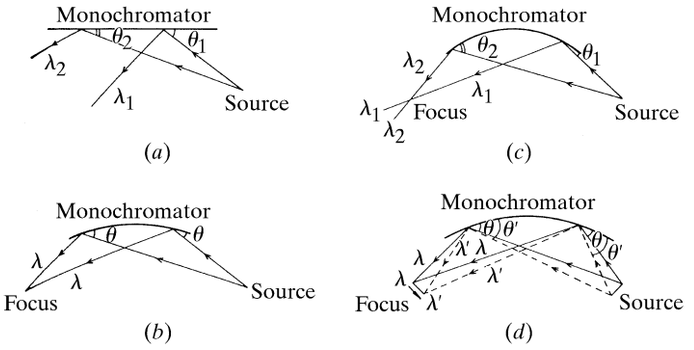

Fig. 8.1.7.1. Single-crystal monochromator illuminated by SR. (*a*) Flat crystal. (*b*) Guinier setting. (*c*) Overbent crystal. (*d*) Effect of source size (shown at the Guinier setting for clarity). From Helliwell (1984). Reproduced with the permission of the Institute of Physics.

gradual change in the photon wavelength selected from the white beam as the length of the monochromator is traversed (Fig. 8.1.7.1*a*). For a point source and a curved monochromator crystal, one specific curvature can compensate for this variation in incidence angle (Fig. 8.1.7.1*b*). The reflected spectral bandwidth is then at a minimum; this setting is known as the 'Guinier position'. If the curvature of the monochromator crystal is increased further, a range of photon wavelengths, $(\delta\lambda/\lambda)_{\rm corr}$, is selected along its length so that the rays converging towards the focus have a correlation of photon wavelength and direction (Fig. 8.1.7.1*c*). The effect of a finite source is to cause a change in incidence angle at the monochromator crystal, so that at the focus there is a photon-wavelength gradient across the width of the focus (for all curvatures) (Fig. 8.1.7.1*d*). The use of a slit in the focal plane is akin to placing a slit at the tangent point to limit the source size.

8.1.7.2.2. *Double-crystal monochromator*

The double-crystal monochromator with two parallel or nearly parallel perfect crystals of germanium or silicon is a common configuration. The advantage of this is that the outgoing monochromatic beam is parallel to the incoming beam, although it is slightly displaced vertically by an amount $2d\cos\,\theta$, where d is the perpendicular distance between the crystals and θ is the monochromator Bragg angle (unless the second crystal is unconnected to the first, in which case it can be translated as well to compensate for that). The monochromator can be rapidly tuned, since the diffractometer or camera need not be re-aligned

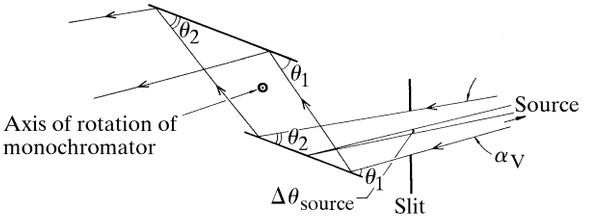

Fig. 8.1.7.2. Double-crystal monochromator illuminated by SR. The contributions of the source divergence, α_V [less than or equal to γ^{-1}, equation (8.1.2.4), depending on the monochromator vertical entrance slit aperture; see also Colapietro *et al.*, 1992], and angular source size, $\Delta\theta_{\rm source}$, to the range of energies reflected by the monochromator are shown. From Helliwell (1984). Reproduced with the permission of the Institute of Physics.

significantly in a scan across an absorption edge. Since the rocking width of the fundamental is broader than the harmonic reflections, the strict parallelism of the pair of the crystal planes can be relaxed or 'detuned', so that the harmonic can be rejected with little loss of the fundamental intensity. The spectral spread in the reflected monochromatic beam is determined by the source divergence accepted by the monochromator, the angular size of the source and the monochromator rocking width (see Fig. 8.1.7.2). The double-crystal monochromator is often used with a toroidal focusing mirror; the functions of monochromatization are then separated from the focusing (Hastings *et al.*, 1978).

8.1.7.2.3. *Crystal sample rocking width*

The rocking width of a reflection depends on the horizontal and vertical beam divergence or convergence (after due account for collimation is taken), γ_H and γ_V, the spectral spreads $(\delta\lambda/\lambda)_{\rm conv}$ and $(\delta\lambda/\lambda)_{\rm corr}$, and the mosaic spread, η. We assume that the mosaic spread η is $\gg\omega$, the angular broadening of a reciprocal-lattice point (relp) due to a finite sample. In the case of synchrotron radiation, γ_H and γ_V are usually widely asymmetric. On a conventional source, usually $\gamma_H \simeq \gamma_V$. Two types of spectral spread occur with synchrotron (and neutron) sources. The term $(\delta\lambda/\lambda)_{\rm conv}$ is the spread that is passed down each incident ray in a divergent or convergent incident beam; the subscript refers to the conventional source type. This is because it is similar to the $K\alpha_1, K\alpha_2$ line widths and separation. At the synchrotron, this component also exists and arises from the monochromator rocking width and finite-source-size effects. The term $(\delta\lambda/\lambda)_{\rm corr}$ is special to the synchrotron or neutron case. The subscript 'corr' refers to the fact that the ray direction can be correlated with the photon or neutron wavelength. In this most general case, and for one example of a $(\delta\lambda/\lambda)_{\rm corr}$ arising from the horizontal ray direction correlation with photon energy and the case of a horizontal rotation axis, the rocking width φ_R of an individual reflection is given by

$$\varphi_R = \left\{L^2\left[(\delta\lambda/\lambda)_{\rm corr}d^{*2} + \zeta\gamma_H\right]^2 + \gamma_V^2\right\}^{1/2} + 2\varepsilon_s L, \qquad (8.1.7.8)$$

where

$$\varepsilon_s = (d^*\cos\theta/2)\left[\eta + (\delta\lambda/\lambda)_{\rm conv}\tan\theta\right] \qquad (8.1.7.9)$$

and L is the Lorentz factor, $1/\left(\sin^2 2\theta - \zeta^2\right)^{1/2}$.

The Guinier setting of an instrument (curved crystal monochromator case, Fig. 8.1.7.1*b*) gives $(\delta\lambda/\lambda)_{\rm corr} = 0$. The equation for φ_R then reduces to

$$\varphi_R = L\left[\left(\zeta^2\gamma_H^2 + \gamma_V^2/L^2\right)^{1/2} 2\varepsilon_s\right] \qquad (8.1.7.10)$$

(from Greenhough & Helliwell, 1982). For example, for $\zeta = 0$, $\gamma_V = 0.2$ mrad (0.01°), $\theta = 15°$, $(\delta\lambda/\lambda)_{\rm conv} = 1\times10^{-3}$ and $\eta =$ 0.8 mrad (0.05°), then $\varphi_R = 0.08°$. But φ_R increases as ζ increases [see Greenhough & Helliwell (1982), Table 5]. In the rotation/oscillation method as applied to protein and virus crystals, a small angular range is used per exposure. For example, the maximum rotation range per image, $\Delta\varphi_{\rm max}$, may be 1.5° for a protein and 0.4° or so for a virus. Many reflections will be only partially stimulated over the exposure. It is important, especially in the virus case, to predict the degree of penetration of the relp through the Ewald sphere. This is done by analysing the interaction of a spherical volume for a given relp with the Ewald sphere. The radius of this volume is given by

$$E \simeq \varphi_R/2L \qquad (8.1.7.11)$$

(Greenhough & Helliwell, 1982).

In Fig. 8.1.7.3, the relevant parameters are shown. The diagram shows $(\delta\lambda/\lambda)_{\rm corr} = 2\delta$ in a plane, usually horizontal with a

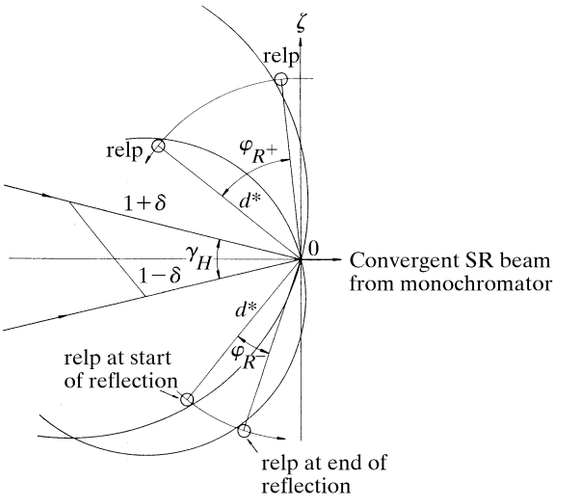

Fig. 8.1.7.3. The rocking width of an individual reflection for the case of Fig. 8.1.7.1(*c*) and a vertical rotation axis. From Greenhough & Helliwell (1982). Copyright (1982) International Union of Crystallography.

perpendicular (vertical) rotation axis, whereas the formula for φ_R above is for a horizontal axis. This is purely for didactic reasons since the interrelationship of the components is then much clearer.

8.1.8. Scientific utilization of SR in protein crystallography

There are a myriad of applications and results of the use of SR in crystallography. Helliwell (1992) has produced an extensive survey and tabulations of SR and macromolecular crystallography applications; Chapter 9 therein concentrates on anomalous scattering and Chapter 10 on high resolution, large unit cells, small crystals, weak scattering efficiency and time-resolved data collection. The field has expanded so dramatically, in fact, that an equivalent survey today would be vast. Table 8.1.4.1 lists the home pages of the facilities, where the specifications and details of the beamlines can be found (*e.g.* all the publications at Daresbury in the protein crystallography area, commencing with NINA in 1976, are to be found at http://www.dl.ac.uk/srs/px/publications.html). The examples below cite extreme cases of the largest unit cell (virus and

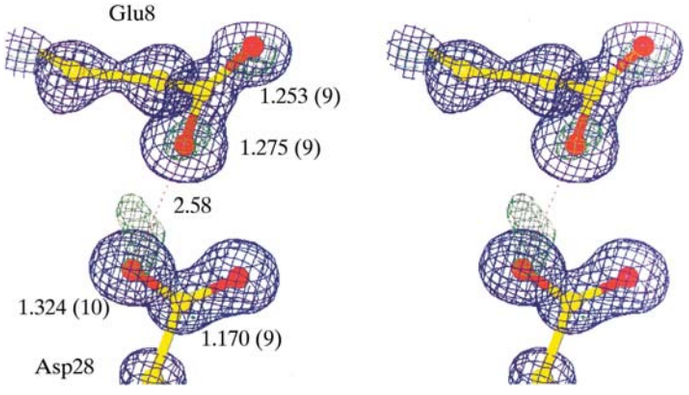

Fig. 8.1.8.1. Determination of the protonation states of carboxylic acid side chains in proteins *via* hydrogen atoms and resolved single and double bond lengths. After Deacon *et al.* (1997) using CHESS. Reproduced by permission of The Royal Society of Chemistry.

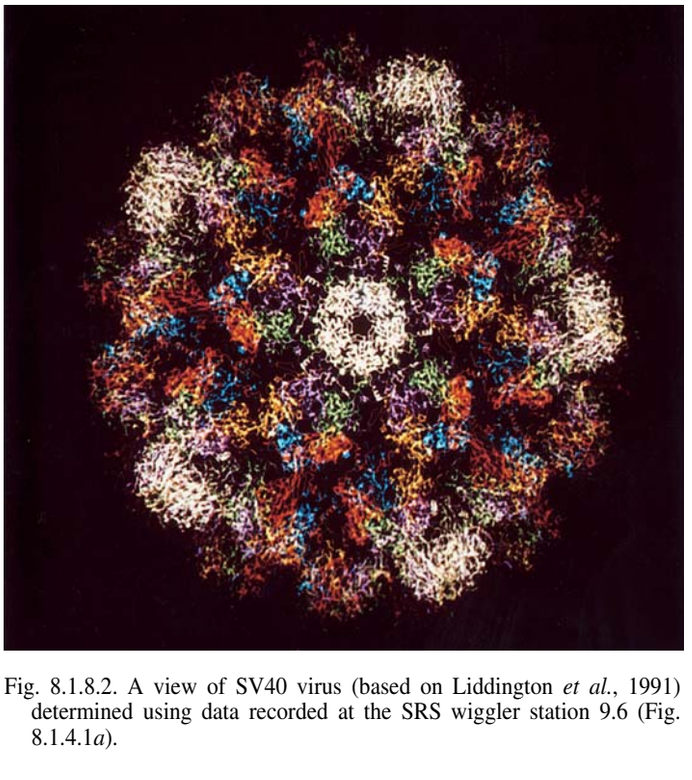

Fig. 8.1.8.2. A view of SV40 virus (based on Liddington *et al.*, 1991) determined using data recorded at the SRS wiggler station 9.6 (Fig. 8.1.4.1*a*).

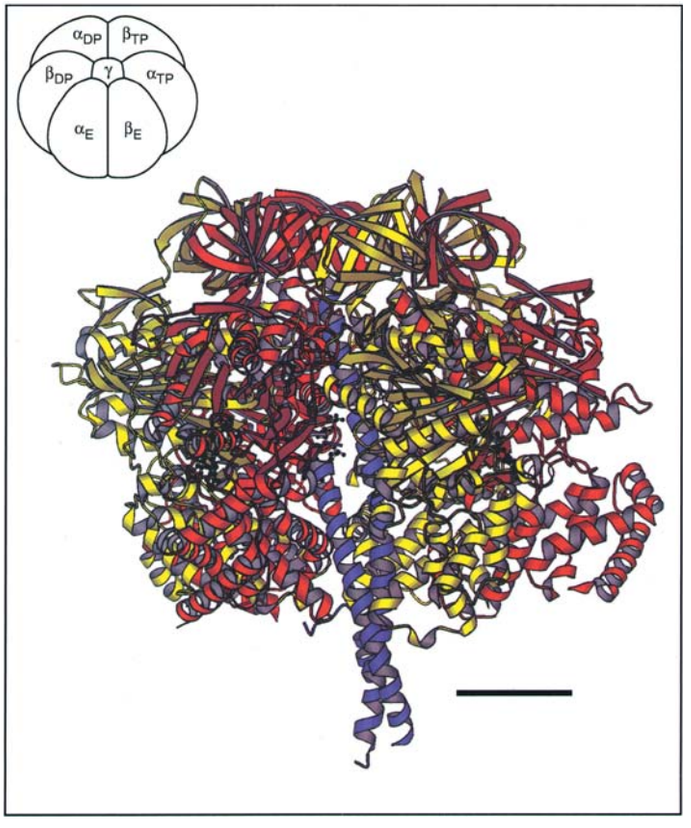

Fig. 8.1.8.3. The protein crystal structure of F_1 ATPase, one of the largest non-symmetrical protein structure complexes, solved using SR data recorded at the SRS wiggler 9.6, Daresbury. The scale bar is 20 Å long. Reprinted with permission from *Nature* (Abrahams *et al.*, 1994). Copyright (1994) MacMillan Magazines Limited.

references